

Variational Physics-Informed Ansatz for Reconstructing Hidden Interaction Networks from Steady States

Kaiming Luo

School of Information Science and Technology, Fudan University, Shanghai, 200438, China

(Dated: Received: date 17 December 2025)

The interaction structure of a complex dynamical system governs its collective behavior, yet existing reconstruction methods struggle with nonlinear, heterogeneous, and higher-order couplings—especially when only steady states are observable. We propose a *Variational Physics-Informed Ansatz* (VPIA) that infers general interaction operators directly from heterogeneous steady-state data. VPIA embeds dynamical symmetries into a differentiable variational representation and reconstructs the underlying couplings by minimizing a physics-derived steady-state residual, without requiring temporal trajectories, derivative estimation, or supervision. Residual sampling combined with natural-gradient optimization enables scalable learning of large and higher-order networks. Across diverse nonlinear systems, VPIA accurately recovers directed, weighted, and multi-body structures under substantial noise, offering a unified and robust framework for physics-constrained inference of complex interaction networks, potentially applicable to biological or social systems where only snapshots are available.

I. INTRODUCTION

The macroscopic behavior of complex systems is fundamentally shaped by their underlying interaction structure^{1,2}. Across neural circuits, ecological communities, gene regulatory networks, power grids, and many-body physical systems, the pattern and strength of interactions govern stability, synchronization, information propagation, and emergent collective phenomena^{3–6}. In many real-world settings, these interactions are directional, weighted, heterogeneous, nonlinear, and may involve higher-order couplings that cannot be reduced to pairwise links. Accurately reconstructing such interaction operators from data is therefore crucial for understanding, predicting, and controlling large-scale dynamical systems.

Although numerous reconstruction techniques perform exceptionally well within the regimes they target⁷, widely used approaches encounter persistent challenges when confronted with noise, nonlinearities, restricted observability, or higher-order structure. Classical time-series-based schemes^{8–10} rely on dense temporal trajectories to estimate derivatives or build local regression models, and their accuracy deteriorates under measurement noise, sparse sampling, latent variables, or when only steady states are experimentally accessible. Recent methods addressing nonlinear or multi-body interactions¹¹ underscore the importance of higher-order couplings but still require high-resolution temporal data. Model-selection and Minimum Description Length (MDL)-based formulations, as well as equilibrium-state approaches^{12–15}, offer elegant inference principles but often rely on tractable analytical forms, linearization, or strong structural priors. Scalability further restricts practical deployment: many representative algorithms exhibit at least cubic computational complexity and rely on sparsity assumptions that break down for dense, weighted, or higher-order networks^{16–23}. As a result, no

existing framework simultaneously satisfies the requirements of generality, robustness, steady-state applicability, and scalability demanded by real-world systems.

The convergence of machine learning with physics-based modeling offers a promising route to address these limitations. Physics-informed learning incorporates physical constraints—such as invariants, conservation laws, and steady-state equations—directly into differentiable architectures^{24–27}. Interpretable model-discovery frameworks²² and Bayesian formulations of network inference^{28,29} further demonstrate how expressive parameterizations and principled inductive biases can yield robust, data-efficient reconstructions. These advances suggest that variational, constraint-driven learning may overcome longstanding challenges associated with noise, nonlinear dynamics, and the absence of temporal trajectories.

In this work, we introduce a steady-state-driven *Variational Physics-Informed Ansatz* (VPIA) for reconstructing general interaction structures from heterogeneous steady-state measurements. Whereas conventional physics-informed neural networks primarily address forward simulation or parameter estimation, VPIA tackles the inverse problem in which the interaction operator itself is unknown and must be inferred from steady-state data. The operator is represented as a trainable variational object whose parameters are optimized to satisfy all steady-state constraints simultaneously. This differentiable formulation naturally accommodates undirected, directed, weighted, and higher-order (multi-body or simplex-level) interactions within a unified representation, while avoiding the need for temporal trajectories or derivative estimation.

To achieve scalability, VPIA integrates residual sampling with natural-gradient optimization. Residual sampling evaluates only a random subset of steady-state constraints at each iteration, reducing computational cost from quadratic dependence on system size to nearly

linear scaling while preserving reconstruction accuracy. Natural-gradient updates exploit the information geometry of the variational parameterization, providing stable and efficient optimization in high-dimensional, highly correlated parameter spaces—particularly for dense graphs and higher-order interaction tensors. Together, these components enable accurate reconstruction on networks with thousands of nodes and complex interaction orders.

Extensive numerical experiments demonstrate that VPIA achieves consistently high reconstruction accuracy across diverse dynamical systems, including phase oscillators, limit-cycle and excitable models, and chaotic dynamics. The method exhibits strong robustness to measurement noise, dynamical noise, and structural perturbations, and its performance improves systematically as more steady states become available, reflecting the global consistency encoded in steady-state constraints. By combining differentiable parameterization, physical structure, sampling-based acceleration, and natural-gradient optimization, VPIA provides a unified, scalable, and noise-resilient framework for reconstructing directed, weighted, and higher-order interaction structures at scales previously inaccessible.

II. VARIATIONAL PHYSICS-INFORMED ANSATZ (VPIA) FRAMEWORK

Understanding the behavior of complex dynamical systems often requires uncovering the structure of their underlying interactions. Steady states obtained under different experimental or driving conditions implicitly encode information about these interactions, providing an opportunity to infer the network topology without relying on full time-series data. Motivated by this observation, we develop a general steady-state-driven framework for network reconstruction, which infers interaction structures from multiple heterogeneous steady-state observations. The framework is general with respect to the dynamical equations, coupling forms, or interaction orders, and applies broadly to systems ranging from oscillator networks to biochemical or ecological dynamics. A conceptual illustration of the overall method is shown in Fig. 1.

A. Problem Setup and Interaction Structures. As illustrated in Fig. 1A, the reconstruction task begins with an unknown interaction network governing an N -node dynamical system. The underlying structure may be undirected, directed, weighted, sparse, or higher-order (e.g., simplicial interactions). Only node-level states and driving conditions are observable; all interaction patterns, weights, and directions are treated as unknown quantities to be reconstructed.

B. Generation of Heterogeneous Steady-State Observations. The sampling stage, depicted in Fig. 1B, proceeds as follows. For each trial m , the system evolves

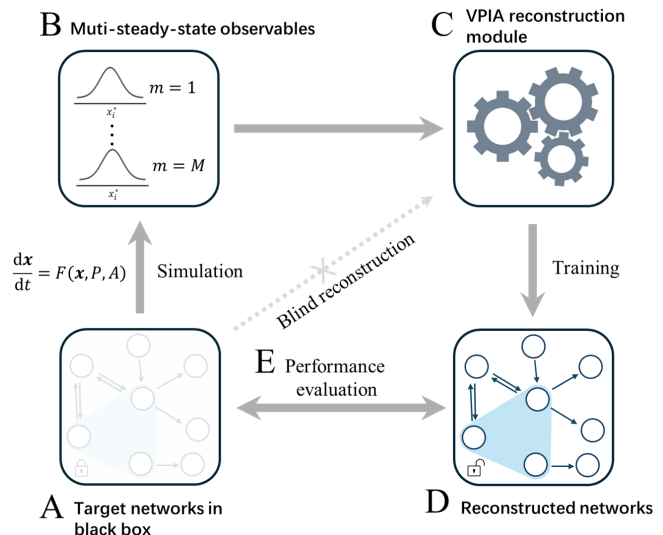


FIG. 1. **Overview of the proposed VPIA framework for network reconstruction.** (A) Ground-truth interaction structure to be reconstructed (not accessible to the reconstruction module). The framework applies broadly to undirected, directed, weighted, sparse, and higher-order interaction patterns; the panel shows a representative example. The light blue shaded region denotes a representative 2-simplex, illustrating a triadic interaction among three nodes. (B) Collection of heterogeneous steady-state observations generated under different intrinsic parameters or driving conditions. Each trial m evolves toward a stable configuration $x^{*(m)}$, which serves as an informative sample for structural inference. (C) Variational representation and physics-informed optimization. The module receives only the observed steady states and remains *blind* to the true network. Each candidate interaction is assigned a trainable variational parameter, mapped to $[0, 1]$ via a sigmoidal ansatz. The formulation naturally accommodates undirected, directed, weighted, and higher-order (e.g., simplex-level) interactions. (D) Reconstructed network \hat{A} obtained by optimizing the variational operator to satisfy all steady-state constraints. (E) Performance evaluation comparing \hat{A} with the ground-truth network A using quantitative metrics—with AUC used as the primary measure of reconstruction fidelity.

under dynamics

$$\dot{x}_i = F_i(x_1, \dots, x_N; p^{(m)}, A), \quad (1)$$

until it reaches a stable steady state denoted abstractly as

$$x^{*(m)} = \Phi(p^{(m)}, A), \quad (2)$$

where $\Phi(\cdot)$ represents the (possibly unknown) steady-state map. By probing the system under distinct intrinsic parameters or driving conditions $\{p^{(m)}\}_{m=1}^M$, we obtain a heterogeneous collection of steady states $\{x^{*(m)}\}_{m=1}^M$. Diversity among these steady states is essential; if all trajectories converge to a synchronized or otherwise degen-

erate configuration, the reconstruction problem becomes unidentifiable.

In practice, steady states that collapse onto a nearly synchronized or otherwise degenerate manifold are discarded. To ensure that each retained steady state carries nontrivial structural information, we require a minimum dispersion level $D(x^{*(m)}) > \epsilon_{\text{sync}}$, where D denotes a simple dispersion measure such as the variance or the mean pairwise distance among node states. This lightweight filtering applies uniformly across oscillatory, excitable, chaotic, and general nonlinear systems.

C. Variational Representation and Physics-Informed Optimization. The core VPIA module shown in Fig. 1C receives only the observed steady states $\{x^{*(m)}\}$ and remains *blind* to the ground-truth interaction structure A , as indicated by the blocked arrow. To infer the unknown topology, we introduce a variational parameterization \mathbf{A}_b in which each candidate interaction is assigned a trainable parameter. A sigmoidal mapping constrains unweighted interactions to the interval $[0, 1]$, ensuring differentiability while preserving topological interpretability. Weighted edges are captured directly through the continuous entries of \mathbf{A}_b . Symmetry constraints impose undirected interactions, independent parameters represent directed ones, and tensor-valued extensions generalize the formulation to higher-order (e.g., 2-simplex) couplings.

The reconstructed adjacency is obtained by minimizing the physics-informed steady-state residual. Given \mathbf{A}_b , each steady-state observation $x^{*(m)}$ yields a node-wise residual

$$R^{(m)} = F\left(x^{*(m)}, p^{(m)}, \mathbf{A}_b\right), \quad (3)$$

and the reconstruction loss aggregates residuals across all nodes and experimental conditions:

$$L = \frac{1}{MN} \sum_{m=1}^M \sum_{i=1}^N (R_i^{(m)})^2. \quad (4)$$

Because the formulation is fully differentiable, the variational operator \mathbf{A}_b is optimized using standard gradient-based methods such as Adam, yielding the estimated adjacency \hat{A} .

Scalability via stochastic residual sampling. As suggested by Fig. 1, the computational cost of evaluating all N residuals at every iteration becomes prohibitive for large networks. VPIA mitigates this bottleneck through stochastic residual sampling, in which only a random subset $S \subseteq \{1, \dots, N\}$ is used during each update:

$$\tilde{L} = \frac{1}{|S|M} \sum_{m=1}^M \sum_{i \in S} (R_i^{(m)})^2. \quad (5)$$

This unbiased estimator reduces the per-iteration complexity from $\mathcal{O}(N)$ to $\mathcal{O}(|S|)$, enabling computationally efficient reconstruction even for large, dense, or higher-order networks.

D. Reconstruction Output. The final stage of the framework, illustrated in Fig. 1D, yields the reconstructed interaction structure \hat{A} obtained from the optimized variational operator. This reconstructed adjacency encapsulates the full set of inferred pairwise or higher-order couplings, providing a direct structural estimate that can be visualized, thresholded, or further analyzed depending on the application. In particular, the continuous entries of \hat{A} encode graded interaction strengths, while their relative ordering serves as the basis for threshold-independent performance metrics.

E. Performance Evaluation. To assess reconstruction fidelity, \hat{A} is systematically compared with the ground-truth network A (Fig. 1E). Standard evaluation metrics—such as the area under the ROC curve (AUC), accuracy, precision, recall, and F1-score—are used to quantify how well the inferred interactions recover the true connectivity pattern. Among these, AUC serves as the primary performance indicator throughout this work because it provides a threshold-independent measure of structural recovery and remains robust across networks with different sparsities.

These metrics characterize reconstruction quality across a broad spectrum of conditions, including different network types (undirected, directed, weighted, and higher-order), varying noise levels, and a wide range of system sizes. The resulting performance profiles provide a comprehensive assessment of the robustness, generality, and scalability of the VPIA framework, which are examined in detail in the subsequent sections.

III. RESULTS

A. Performance on Artificial Networks

To assess the reconstruction framework under controlled conditions, we examine ensembles of artificial networks and evaluate the consistency of the inferred interaction patterns. Across all realizations considered, the method achieves highly reliable recovery of the underlying connectivity. The rapid improvement in discrimination performance, illustrated in Fig. 2B, reflects the substantial information encoded in steady-state responses and the efficiency with which the framework extracts structural signatures from them.

The robustness of the approach extends across qualitatively distinct dynamical regimes. As indicated by the broad collection of models summarized in the inset of Fig. 2B, reconstruction accuracy remains consistently high for phase-oscillator systems, amplitude-mediated oscillators, and paradigmatic chaotic flows alike. This insensitivity to dynamical class suggests that the reconstruction mechanism relies on invariants that persist irrespective of whether the underlying dynamics are chaotic or non-chaotic.

The scaling characteristics of the framework further

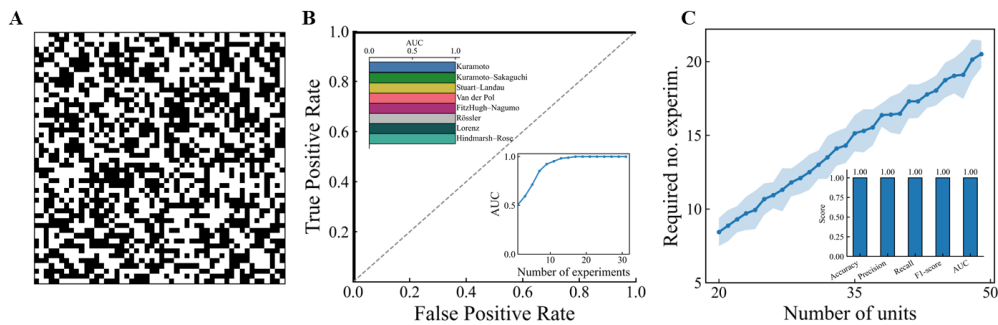


FIG. 2. **Reconstruction performance of the proposed VPIA framework.** (A) Ground-truth adjacency matrix of a representative undirected network, where black and white entries denote the presence and absence of links, respectively. (B) Receiver operating characteristic (ROC) curve obtained from steady-state data generated by Kuramoto dynamics. The upper-left inset reports the AUC achieved across eight distinct dynamical systems (Kuramoto, Kuramoto–Sakaguchi, Stuart–Landau, Van der Pol, FitzHugh–Nagumo, Rössler, Lorenz, and Hindmarsh–Rose), demonstrating model-independent reconstruction accuracy. The lower-right inset shows the AUC as a function of the number of heterogeneous steady-state experiments M , indicating rapid convergence toward perfect discrimination. (C) Minimum number of experiments required for successful reconstruction as a function of network size N . Each point corresponds to an average over 20 independent realizations, with shaded bands indicating standard deviations. Successful reconstruction is defined as simultaneously achieving $AUC = 1$ and perfect binary classification (Accuracy, Precision, Recall, and F1-score all equal to 1).

support its applicability to increasingly large systems. The approximate linear dependence between the number of required steady states and network size, shown in Fig. 2C, indicates that the informational yield per experiment remains stable as dimensionality increases. This near-linear trend, observed across independent realizations, highlights the favorable scaling profile of the method and its suitability for large-scale applications. Supplementary Sec. S2 provides a rigorous proof that a finite number of steady states is sufficient to guarantee identifiability of the underlying interaction structure, and establishes the corresponding information-theoretic upper bound.

The generality of the framework extends beyond the specific network realization displayed in Fig. 2A. High reconstruction fidelity is maintained across networks spanning a broad sparsity spectrum—from highly sparse graphs to relatively dense connectivity patterns. As detailed in Supplementary Sec. S3, VPIA maintains uniformly high reconstruction accuracy across scale-free, small-world networks, and random graphs, and further extends reliably to directed and weighted interaction structures. Together, these results demonstrate that the reconstruction strategy captures universal structural features and remains resilient across diverse topological and dynamical settings.

Beyond these structural and dynamical tests, we further benchmark VPIA against a suite of classical reconstruction approaches, as summarized in Supplementary Sec. S4. We compare only with methods that operate under the same type of data (steady states or dynamical trajectories), while methods requiring observed networks or network ensembles are not applicable in this setting. The comparison includes information-theoretic and regression-based methods such as transfer entropy (TE),

network deconvolution (ND)³⁰, partial phase synchronization (PPS)³¹, modular response analysis (MRA)³², global silencing (GS)³³, and correlation-based inference. Despite their diverse methodological foundations—ranging from Jacobian regression and covariance inversion to indirect-interaction filtering—these baselines consistently exhibit degraded performance when networks become moderately dense, directed, weighted, or nonlinear in their steady-state mappings. In contrast, VPIA achieves uniformly high AUC and near-perfect support recovery across all tested regimes, highlighting its scalability, numerical stability, and superior identifiability relative to existing state-of-the-art methods.

B. Noise Robustness and Perturbation Tolerance

To evaluate the robustness of the VPIA framework, we tested its network reconstruction performance under three representative types of zero-mean random noise, as illustrated in Fig. 3. Observation noise (Fig. 3A) refers to additive errors directly superimposed on the measured steady-state data. Dynamical noise (Fig. 3B) represents the intrinsic stochastic fluctuations in the system’s internal dynamical process, i.e., a random term introduced into the governing differential equations that determine the state evolution. Network noise (Fig. 3C) simulates inherent uncertainties or minor structural perturbations in the true interaction network itself.

The reconstruction curves on the right side of Fig. 3 demonstrate that VPIA maintains excellent performance under all noise conditions. For moderate noise levels, only $\mathcal{O}(N)$ steady-state samples are required to achieve high-accuracy recovery ($AUC > 95\%$). Even under strong noise (e.g., level 0.5), the reconstruction accu-

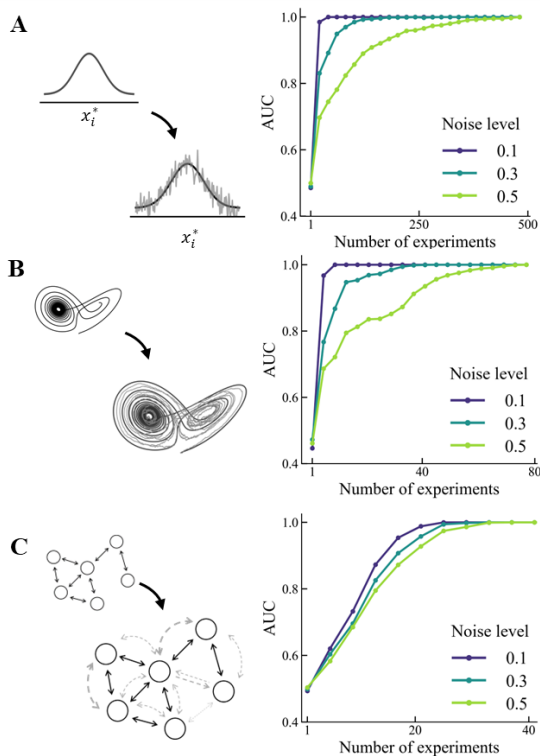


FIG. 3. **Robustness of the VPIA framework under three types of zero-mean random noise.** (A) Observation noise, where each measured steady-state is contaminated by additive random fluctuations. (B) Dynamical noise, arising from intrinsic stochastic variations during the system’s evolution, modeled as a random term added to the governing differential equations. (C) Network noise, representing structural uncertainties or small perturbations in the underlying adjacency matrix. For each noise type, three representative noise strengths are examined, as shown in the right-hand panels. Across all noise levels, the reconstruction accuracy of the VPIA framework improves steadily as the number of steady-state experiments increases, ultimately approaching nearly perfect performance ($\text{AUC} \rightarrow 1$). All results are averaged over 20 independent realizations.

accuracy continues to improve as the sample size increases. This confirms that high-quality network reconstruction remains attainable under severe interference, provided a sufficient number of steady-state observations are available.

This robustness originates from the disparity between the global-constraint nature of the steady-state equations and the local, zero-mean character of the noise. Each steady-state observation imposes a globally coupled constraint on all node variables, whereas each type of noise acts as a local perturbation. As the number of samples grows, the perturbations are averaged out within the framework of global constraints, allowing the optimization to converge to the consistent physical relationships underlying the data. A formal analysis of this concentration effect, including robustness under measurement, dynamical, and structural noise, is provided in Supple-

mentary Sec. S5 .

Notably, network noise (Fig. 3C) presents a more fundamental challenge: it not only obscures the true network to be inferred at its source but can also break the intrinsic symmetry and consistency that should exist among different steady-state datasets. Nevertheless, VPIA exhibits strong robustness even under such noise, highlighting the method’s ability to overcome the fundamental difficulty posed by structural uncertainty by integrating the deep common constraints embedded in multiple steady-state observations.

C. Reconstruction on Large and Realistic Networks

In many real-world systems, the underlying networks can be remarkably large, often reaching up to the order of 10^3 nodes in gene regulatory networks, neural circuits, power-grid infrastructures, or social-interaction layers. Such large scales render the computational complexity of structural inference prohibitive for many traditional reconstruction approaches, especially those relying on exhaustive search, full-batch evaluation, or global combinatorial scans. As a consequence, numerous classical methods fail once the network size approaches even a few hundred nodes. Thus, achieving practical scalability while preserving high reconstruction accuracy becomes essential for enabling real-world applications.

In our framework, the dominant computational cost arises from training the steady-state residuals. For each observed steady state $m = 1, \dots, M$, the system provides N constraints $F_i(x^{*(m)}, p^{(m)}, A) = 0$, resulting in a total of MN node–state residuals. A naïve full-batch update would therefore require $O(MN)$ evaluations per iteration, which becomes increasingly expensive as M and N grow. To address this scaling bottleneck, we employ a residual sampling strategy that selects only a small random subset of the MN residuals at each iteration. This reduces the per-iteration complexity to $O(N)$ and enables reconstruction on substantially larger networks.

A key advantage of this sampling-based design is its applicability to both sparse and dense real-world networks. Many large-scale systems—such as social, biological, and infrastructural networks—are highly sparse, where each residual depends only on $O(k)$ local interactions with $k \ll N$. In such cases, even a modest number of sampled node–state pairs suffices to obtain an accurate and low-variance estimate of the full residual. At the same time, certain empirical networks—including functional brain networks, economic correlation structures, and multilayer interaction systems—exhibit moderate or even high density. For these networks, evaluating all interactions explicitly would lead to quadratic computational cost, whereas residual sampling decouples the per-iteration complexity from network density and keeps it linear in N . Thus, sampling serves not merely as an acceleration technique, but as a unifying mechanism that ensures scalable reconstruction across both sparse and

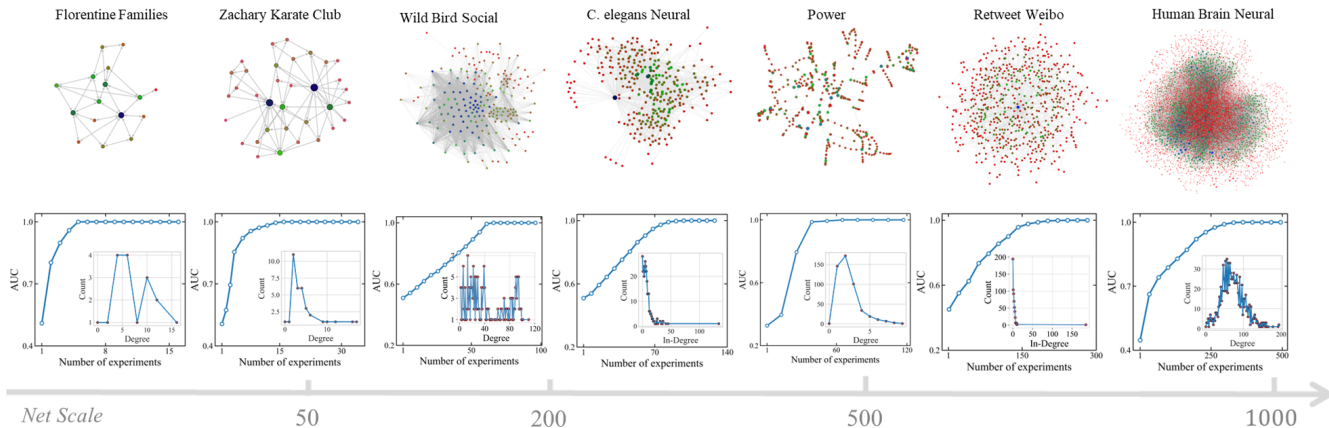


FIG. 4. **Reconstruction performance of VPIA across real-world networks of increasing scale.** Shown from left to right are six representative networks spanning over three orders of magnitude in size. Top panels display the network structures, visualized with node colors indicating degree (or in-degree for directed networks). Bottom panels show the reconstruction accuracy measured by AUC as a function of the number of steady-state experiments, with each inset depicting the corresponding degree distribution. Across all networks—despite substantial variations in size, topology, and degree heterogeneity—VPIA consistently achieves rapid convergence toward perfect reconstruction, requiring only a modest number of steady-state samples even in large-scale systems (rightmost panels). The results highlight the scalability and broad applicability of VPIA for accurate network inference in real-world settings.

dense regimes.

As the number of parameters grows with network size, standard first-order gradient methods may converge slowly or become unstable due to the anisotropic and often ill-conditioned parameter landscape. Natural gradient (or equivalently stochastic reconfiguration) provides curvature-aware updates that stabilize optimization and complement the sampling strategy in large-scale settings.

To assess the practical performance of the proposed method, we evaluate reconstruction accuracy on several representative large-scale real and synthetic networks. Fig. 4 shows the AUC as a function of the number of observed experiments for real networks (detailed in Tab. I) from the data of Ref.^{34–36} of different sizes. The results demonstrate that the AUC increases rapidly with the number of observed experiments and approaches unity even for networks with up to 10^3 nodes, illustrating that the combination of residual sampling and natural-gradient optimization enables accurate and scalable reconstruction in real-world complex networks.

D. Reconstruction of higher-order interactions

Higher-order interaction networks extend traditional pairwise graphs by allowing multiple nodes to participate in an interaction simultaneously. As illustrated in Fig. 5A, these interaction units, or simplices, include 1-simplex (pairwise edges), 2-simplex (triangles), 3-simplex, and 4-simplex structures, each encoding increasingly complex multi-body relationships. Such higher-order couplings are known to play an essential role in

TABLE I. Real-world network datasets analyzed in this study. For each network, we report its type (directed or undirected), the number of nodes N , number of edges E , and density ρ , defined as $\rho = 2E/[N(N-1)]$ for undirected graphs and $\rho = E/[N(N-1)]$ for directed graphs.

Network	Type	Nodes	Edges	Density
Florentine Families	Undir	16	20	0.1667
Zachary Karate Club	Undir	34	78	0.1390
Les Misérables	Undir	77	254	0.0862
Wild Bird Social	Undir	202	11733	0.5861
C. elegans Neural	Dir	297	2359	0.0259
Power	Undir	494	596	0.0049
Retweet Weibo	Dir	596	1415	0.0080
Human Brain	Undir	989	35730	0.036

diverse systems ranging from neuronal assemblies and biochemical reaction pathways to synchronization processes and collective decision-making. Because the number of possible higher-order interactions grows combinatorially with system size, directly measuring or enumerating them is generally infeasible, making the reconstruction problem fundamentally challenging.

Within the VPIA framework, all candidate multi-body couplings are encoded as variational tensor elements that are jointly optimized by minimizing steady-state residuals. This unified treatment does not require prior knowledge of which interaction orders are present, and it naturally accommodates the simultaneous presence of 1-, 2-, 3-, and 4-simplex structures. A representative recon-

struction is shown in Fig. 5B, where a 2-simplex adjacency tensor of dimension $4 \times 4 \times 4$ is accurately recovered from heterogeneous steady-state observations. The inferred tensor closely matches the ground truth, demonstrating that the higher-order structure leaves identifiable signatures in the steady-state equations that can be effectively exploited by VPIA.

The effect of data abundance is summarized in Fig. 5C. As the number of steady-state experiments increases, the AUC improves rapidly and approaches unity after only a modest number of samples. This behavior indicates that even a small number of sufficiently diverse steady states carries substantial information about the underlying multi-body couplings, enabling accurate reconstruction without requiring temporal trajectories.

Across simplex orders, Fig. 5D shows that the number of required experiments increases with system size, reflecting the enlarged interaction space associated with higher-order couplings. Importantly, however, even for higher-order structures, the required number of steady states grows sub-combinatorially and remains far below the naive dimensionality of the candidate interaction space. This indicates that VPIA continues to satisfy the reconstruction requirements in genuinely higher-order regimes, leveraging global physical consistency to avoid the combinatorial blow-up that would otherwise arise in such settings.

Although the number of candidate higher-order interactions grows combinatorially with N , the computational cost of VPIA does not. Residual sampling ensures that each optimization step evaluates only $O(N)$ constraints, making the per-iteration complexity effectively independent of the combinatorial parameter space.

Finally, robustness under realistic uncertainties is shown in Fig. 5E, which reports reconstruction accuracy under observation noise, dynamical noise, and structural noise at multiple amplitudes. In all three cases, AUC improves steadily with additional steady states, and accurate reconstruction is restored once enough independent conditions are sampled. This resilience highlights an important advantage of the method: the steady-state equations encode global consistency conditions that suppress random fluctuations and enable stable inference even under significant noise.

Together, the results in Fig. 5A–E demonstrate that VPIA can reliably recover 1- through 4-simplex interaction structures from steady-state data alone. The framework exhibits strong robustness to multiple forms of noise, scales efficiently with system size and simplex order, and accurately resolves multi-body interaction tensors without requiring temporal information or prior structural assumptions.

IV. DISCUSSION

The Variational Physics-Informed Ansatz (VPIA) presented here offers a general and physically grounded

framework for reconstructing interaction structures in complex dynamical systems using heterogeneous steady-state observations. In contrast to approaches based on statistical correlations, temporal derivatives, or explicit parametric modeling of the governing equations, VPIA incorporates the steady-state conditions directly into a differentiable variational operator. This formulation places physical consistency at the center of the reconstruction task and enables the extraction of structural information that persists across diverse dynamical regimes, noise levels, and system sizes.

It is important to clarify that VPIA is fundamentally distinct from classical physics-informed neural networks. Whereas traditional PINNs assume known governing equations and infer latent variables or parameters, VPIA treats the entire interaction operator as an unknown variational object. The method therefore solves an inverse operator-learning problem rather than a PDE-solving task, which places it outside the scope of standard PINN formulations.

A major advantage of the framework lies in its representational flexibility. Each potential interaction is assigned a trainable variational parameter, enabling a unified treatment of undirected, directed, and weighted networks through sigmoidal or continuous mappings. This generality is particularly relevant in real-world systems where directionality, weight heterogeneity, and mixed structural motifs often coexist and cannot be predetermined *a priori*.

Equally important is the method’s model-agnostic behavior. VPIA achieves consistently high accuracy across phase oscillators, limit-cycle systems, excitable media, and chaotic flows, despite their strongly differing dynamical characteristics. This observation suggests that the essential information governing structural inference is encoded in the steady-state configurations themselves, rather than in full dynamical trajectories or specific functional forms. The ability to rely solely on steady-state data offers a practical and minimally intrusive route for experimental applications where dynamics may be unknown or only partially observable.

The framework naturally extends to quasi-steady and metastable states. When the temporal drift of these states is small relative to their spatial dispersion, each observation still imposes an approximate steady-state constraint. As a result, the method remains applicable to systems that do not converge to strict fixed points, broadening its utility in noisy or partially stable experimental environments.

VPIA further exhibits strong robustness to measurement, dynamical, and structural noise. While these noise sources differ in origin, they all act as local perturbations on the observed states, whereas each steady state imposes a global constraint across the network. As additional steady states are incorporated, coherent physical relationships accumulate while random fluctuations are averaged out, explaining the systematic improvement in reconstruction accuracy with sample size.

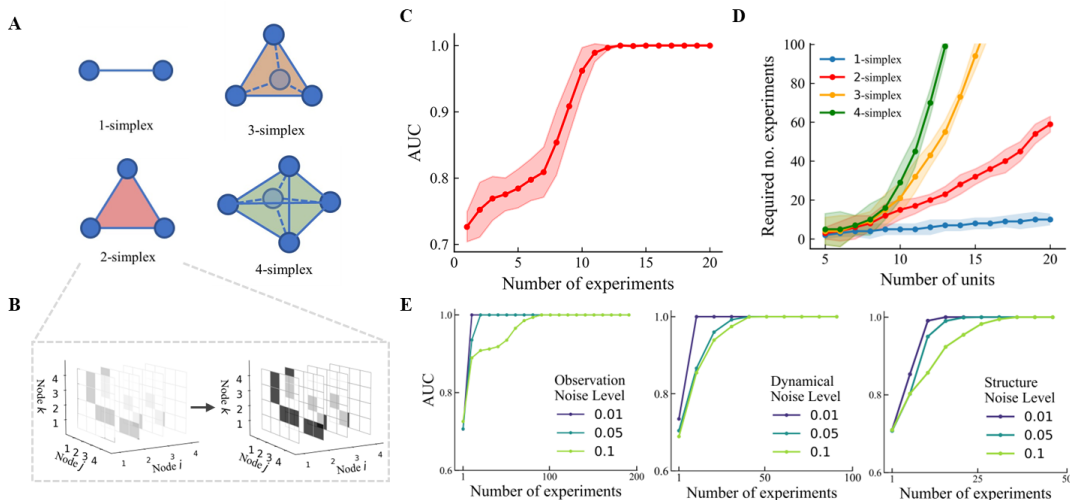


FIG. 5. (A) Illustrations of 1-, 2-, 3-, and 4-simplex interaction motifs, representing pairwise, triangular, tetrahedral, and four-body coupling structures. (B) Example reconstruction of a 2-simplex adjacency tensor. The left panel shows the ground-truth higher-order tensor, and the right panel displays the corresponding tensor recovered by VPIA. (C) Reconstruction accuracy measured by AUC as a function of the number of steady-state experiments, showing rapid improvement and saturation toward perfect reconstruction. (D) Required number of steady-state experiments for successful reconstruction across networks composed of 1-, 2-, 3-, and 4-simplex interactions. Higher-order simplices require substantially more experiments due to the increasing combinatorial complexity of multi-node interactions. (E) Robustness of VPIA under three representative noise sources: observation noise (left), dynamical noise (middle), and structural noise (right). For each noise type, multiple noise amplitudes are tested. Although higher noise levels reduce the initial AUC, accurate reconstruction is still achieved once a sufficient number of steady-state experiments is provided. Panels (C)–(E) use networks with $N = 10$ nodes, where all possible 2-, 3-, and 4-simplex interactions are independently included with probability $p = 0.5$, resulting in dense higher-order interaction structures.

A central strength of the method is its computational scalability. Classical reconstruction approaches often become intractable due to the rapid growth of parameters and constraints in large systems. VPIA mitigates these challenges through residual sampling—which evaluates only a small subset of node-wise constraints—and natural-gradient optimization, which stabilizes updates in high-dimensional and anisotropic parameter spaces. Together, these components enable accurate inference on networks exceeding 10^3 nodes while maintaining computational efficiency.

The variational formulation also extends seamlessly to higher-order structures such as simplicial complexes and general hypergraphs. Although numerical demonstrations focus on lower-order examples, the tensor-based parameterization accommodates interactions of arbitrary order. Residual sampling and natural-gradient updates play an essential role in managing the combinatorial growth of parameters, enabling scalable reconstruction of both pairwise and multi-body interaction structures from steady-state data alone.

Despite its broad applicability, several practical considerations remain. The method requires multiple distinct steady states generated through controlled perturbations or naturally varying conditions; acquiring sufficiently diverse samples may be experimentally challenging. In systems with strong fluctuations or without well-defined steady states, additional preprocessing or mod-

ified formulations may be needed. Finally, while VPIA scales favorably compared with existing approaches, reconstructing extremely large or very high-order simplicial networks may still impose substantial computational demands, motivating future developments in distributed optimization and more efficient variational parameterizations.

V. MATERIALS AND METHODS

A. Dynamical models and steady-state generation

We consider a broad class of networked dynamical systems in which the interaction structure enters explicitly through adjacency objects of potentially multiple orders. Let $x_i \in \mathbb{R}$ denote the state of node i ($i = 1, \dots, N$), $p^{(m)}$ the m -th external driving or experimental condition, and $\{A^{(d)}\}_{d \geq 1}$ a hierarchy of adjacency tensors encoding d -body interactions. The dynamics of node i can be written in the unified form

$$\dot{x}_i = F_i(x; p^{(m)}, \{A^{(d)}\}_{d \geq 1}), \quad (6)$$

where $A_{ij}^{(1)}$ describes pairwise couplings, $A_{ijk}^{(2)}$ corresponds to 2-simplex (triadic) interactions, $A_{ijkl}^{(3)}$ describes

3-simplex interactions, and more generally

$$A^{(d)} \in \mathbb{R}^{N^d}$$

encodes all hyperedges of order d . This tensorial representation provides a unified description of arbitrary mixtures of pairwise and higher-order interactions, making the proposed reconstruction framework directly applicable to general hypergraph and simplicial-complex dynamical systems.

To obtain steady-state observations, the system is initialized under driving condition $p^{(m)}$ from a random transient configuration and integrated numerically using either a fourth-order Runge–Kutta method or an adaptive-step ODE solver. A configuration is regarded as a steady state $x^{*(m)}$ once the convergence criterion

$$\|\dot{x}\|_2 < \varepsilon \quad (7)$$

is met, where $\|\cdot\|_2$ denotes the Euclidean norm. Empirically, a heterogeneous collection of $M = O(N)$ to $O(N \log N)$ steady states provides sufficiently many independent constraints to ensure structural identifiability of the underlying interaction tensors. Steady states that are fully synchronized or otherwise degenerate—and therefore contain no usable structural information—are discarded.

The generality of this formulation with respect to the governing dynamics is assessed by evaluating reconstruction performance across a wide spectrum of canonical oscillator models, as summarized in Fig. 2B. The tested systems include phase-based oscillators (Kuramoto, Kuramoto–Sakaguchi), limit-cycle models (Stuart–Landau, Van der Pol, FitzHugh–Nagumo), and representative chaotic systems (Rössler, Lorenz, Hindmarsh–Rose). Despite the pronounced differences in their dynamical behavior, all these systems yield identical reconstruction accuracy, indicating that the performance of the proposed VPIA framework depends primarily on the information embedded in the steady-state equations rather than the specific form of the time-evolution operator $F_i(\cdot)$. For clarity and without loss of generality, Kuramoto dynamics is adopted for all subsequent numerical experiments.

To illustrate the role of steady states more explicitly, note that each observed steady state $x^{*(m)}$ enforces a set of algebraic constraints

$$F_i(x^{*(m)}; p^{(m)}, \{A^{(d)}\}_{d \geq 1}) = 0, \quad i = 1, \dots, N, \quad (8)$$

which relate the unknown interaction tensors $\{A^{(d)}\}$ to the measured configurations $x^{*(m)}$. Across different driving conditions, these constraints form an overdetermined system whose consistent solution corresponds to the true underlying network structure. This viewpoint clarifies why the method exhibits strong robustness and why diverse dynamical processes lead to identical reconstruction outcomes.

B. Filtering degenerate steady states

Not all steady states provide useful structural information. Configurations that lie close to a low-dimensional degenerate manifold—including fully synchronized states, nearly uniform fixed points, or collectively collapsed configurations—do not reflect the heterogeneity of the underlying interaction structure and must be excluded prior to reconstruction.

To systematically remove such samples, we adopt a lightweight dispersion criterion. Given a steady state $x^{*(m)} = (x_1^{*(m)}, \dots, x_N^{*(m)})$, we define a dispersion measure $D(x^{*(m)})$ as either

$$D_{\text{var}}(x^{*(m)}) = \text{Var}(x^{*(m)}), \quad (9)$$

or the mean pairwise distance

$$D_{\text{mpd}}(x^{*(m)}) = \frac{1}{N(N-1)} \sum_{i \neq j} \|x_i^{*(m)} - x_j^{*(m)}\|. \quad (10)$$

A steady state is accepted if and only if

$$D(x^{*(m)}) > \epsilon_{\text{sync}}, \quad (11)$$

where ϵ_{sync} is a small threshold determining the minimum spread required for informativeness. This filtering applies uniformly across oscillatory, excitable, chaotic, and general nonlinear dynamical systems, and it ensures that each retained steady state contributes independent constraints for accurate network reconstruction.

In all numerical experiments we set ϵ_{sync} in the range 10^{-4} – 10^{-3} , though any value satisfying the scale of the system’s state variables produces similar results.

C. Variational parameterization of adjacency structures

Every potential interaction is associated with a trainable parameter. For pairwise couplings, a parameter θ_{ij} determines the soft adjacency estimate through a scaled sigmoid:

$$\hat{A}_{ij} = \sigma(k\theta_{ij}) = \frac{1}{1 + \exp[-k\theta_{ij}]}, \quad (12)$$

where $k \gg 1$ controls the steepness of the continuous–binary transition. For undirected networks the symmetry constraint $\hat{A}_{ij} = \hat{A}_{ji}$ is enforced, while directed networks keep all entries independent. Weighted networks keep the continuous output without thresholding.

Higher-order interactions are parameterized analogously:

$$\hat{A}_{ijk}^{(2)} = \sigma(k\theta_{ijk}), \quad \hat{A}_{ijkl}^{(3)} = \sigma(k\theta_{ijkl}), \quad (13)$$

yielding a unified variational representation for general simplex- or hypergraph-based structures.

D. Physics-informed variational optimization: residual sampling and natural-gradient updates

Given a variational adjacency estimate \hat{A} , each experimental condition m yields node-wise steady-state constraints

$$R_i^{(m)} = F_i(x^{*(m)}, p^{(m)}, \hat{A}), \quad (14)$$

which vanish for an exact reconstruction. Directly aggregating all MN residuals quickly becomes inefficient for large systems and, critically, for dense or higher-order networks where the number of nontrivial constraints grows combinatorially with N .

Residual sampling. To address the computational cost associated with evaluating all residuals, we adopt residual sampling. At each iteration, a uniformly selected subset

$$S \subset \{1, \dots, N\}, \quad |S| = s \ll N$$

is used to form the stochastic objective

$$\mathcal{L}_{\text{RS}} = \frac{1}{M_s} \sum_{m=1}^M \sum_{i \in S} [R_i^{(m)}]^2. \quad (15)$$

Uniform sampling guarantees unbiasedness, $\mathbb{E}[\mathcal{L}_{\text{RS}}] = \mathcal{L}$, while reducing the per-iteration complexity from $O(MN)$ to $O(Ms)$. This reduction is especially critical in dense pairwise networks and higher-order d -simplices, where the full residual set scales as $O(N^2)$ – $O(N^d)$ and rapidly becomes intractable to evaluate at each step. Even modest sampling ratios ($s/N \sim 5\%$) produce sufficiently low-variance gradient estimates for stable optimization in practice.

Natural-gradient updates. The variational parameters defining the interaction operator, $\{\theta_{ij}, \theta_{ijk}, \dots\}$, reside in a high-dimensional space whose cardinality scales as $P = O(N^2)$ for pairwise networks and $P = O(N^d)$ for d -simplices. The resulting loss landscape is strongly anisotropic and ill-conditioned, severely limiting the efficiency of standard gradient descent. To stabilize convergence, we employ a natural-gradient update,

$$\Delta\theta = -\eta F^{-1} \nabla_{\theta} \mathcal{L}, \quad (16)$$

where F is the Fisher information matrix. Since constructing the full $P \times P$ matrix is infeasible for large-scale systems, we use the diagonal approximation

$$F \approx \text{diag}(\nabla_{\theta} \mathcal{L} \circ \nabla_{\theta} \mathcal{L}), \quad (17)$$

yielding the curvature-aware update

$$\Delta\theta = -\eta \frac{\nabla_{\theta} \mathcal{L}}{\varepsilon + \nabla_{\theta} \mathcal{L} \circ \nabla_{\theta} \mathcal{L}}, \quad (18)$$

with $\varepsilon > 0$ a small regularizer. This reduces the per-iteration complexity from $O(P^3)$ to $O(P)$, enabling tractable optimization for networks with up to $N \sim 10^3$ nodes and for higher-order interaction tensors.

Scalability for large, dense, or higher-order networks. The complementary roles of residual sampling and natural-gradient updates become especially critical in large, dense, or higher-order interaction structures. Residual sampling suppresses the combinatorial growth of steady-state constraints—from MN node-wise relations in pairwise systems to $O(N^d)$ constraints in d -simplicial networks—by evaluating only a small, informative subset at each iteration. In parallel, the diagonal-Fisher natural gradient counteracts the severe ill-conditioning induced by the $O(N^d)$ -dimensional variational parameter space, ensuring stable curvature-aware updates even when interactions are dense or when higher-order tensors dominate the dynamics. Together, these two components enable a scalable and robust physics-informed optimization framework that remains effective for large-scale, dense, weighted, directed, and higher-order networks reconstructed from steady-state data. Additional analysis of the interplay between residual sampling and natural-gradient optimization is provided in Supplementary Sec. S6.

E. Reconstruction evaluation metrics

To evaluate reconstruction quality, we employ the area under the ROC curve (AUC), which metrics characterize different aspects of reconstruction performance, particularly under varying network densities.

To provide a sparsity-insensitive evaluation, we compute the AUC, defined as

$$\text{AUC} = \int_0^1 \text{TPR}(\text{FPR}) d(\text{FPR}), \quad (19)$$

where TPR and FPR denote the true positive and false positive rates under threshold sweeping. AUC depends solely on the ranking of predicted edge strengths \hat{A}_{ij} rather than on their binarized values, and therefore remains informative even for highly sparse networks. Empirically, $\text{AUC} > 0.9$ corresponds to robust structural recovery, indicating that the majority of true edges are consistently ranked above non-edges.

F. Noise models: measurement, dynamical, and structural noise

To systematically assess the robustness of the reconstruction framework under realistic uncertainties, we consider three classes of noise—measurement, dynamical, and structural—which correspond respectively to panels A–C of Fig. 3. All noise terms are modeled as independent, zero-mean Gaussian fluctuations $\xi \sim \mathcal{N}(0, 1)$. For each noise type, a dedicated scale parameter σ_{obs} , σ_{dyn} , or σ_{str} is introduced. These parameters serve as the noise levels that control the magnitude of the corresponding perturbations and provide a dimensionally consistent and physically interpretable formulation.

Observation noise. Uncertainty in measured steady-state values is introduced by perturbing each observed $x_i^{*(m)}$ as

$$\tilde{x}_i^{*(m)} \longrightarrow x_i^{*(m)} + \sigma_{\text{obs}} \text{MAD} \xi_i, \quad \xi_i \sim \mathcal{N}(0, 1). \quad (20)$$

Here σ_{obs} is the observation noise level, and MAD denotes the median absolute deviation of the steady states. The normalization by MAD ensures that σ_{obs} represents a relative fluctuation amplitude; for instance, $\sigma_{\text{obs}} = 0.01$ corresponds to a perturbation of $1\% \times \text{MAD}$.

Dynamical noise. Intrinsic stochasticity during system evolution is modeled as

$$\dot{x}_i = F_i(x; p^{(m)}, A) + \sigma_{\text{dyn}} \xi_i(t), \quad \xi_i(t) \sim \mathcal{N}(0, 1), \quad (21)$$

where σ_{dyn} serves as the dynamical noise level. This term accounts for small random deviations around steady-state behavior due to microscopic randomness, thermal effects, or unresolved environmental interactions. During numerical integration, $\xi_i(t)$ is resampled at each time step to approximate discrete-time white noise.

Structural noise. Variability or uncertainty in the interaction topology is introduced by perturbing the adjacency matrix:

$$\tilde{A}_{ij} \longrightarrow A_{ij} + \sigma_{\text{str}} \xi_{ij}, \quad \xi_{ij} \sim \mathcal{N}(0, 1). \quad (22)$$

Here σ_{str} is the structural noise level, representing errors in network acquisition, fluctuations in connection strength, or temporal variability of interactions. Unless stated otherwise, perturbations are applied only to entries corresponding to existing links.

The noise levels σ_{obs} , σ_{dyn} , and σ_{str} thus provide a unified set of tunable parameters for systematically evaluating the influence of measurement errors, dynamical randomness, and structural uncertainty on network reconstruction performance. For each condition, noise is regenerated independently across nodes, links, and realizations, and all reported results are averaged over 20 independent network instances to ensure statistical reliability.

G. Numerical implementation and synthetic network generation

All synthetic pairwise networks are generated as Erdős–Rényi random graphs $G(N, p)$ with $p = 0.5$, which provide maximum-entropy connectivity without structural bias.

For higher-order experiments, we construct simplicial complexes and hypergraphs directly by combinatorial sampling. Given N nodes, all possible k -node subsets are enumerated for the desired simplex order k , and each candidate simplex is included independently with probability $p = 0.5$. This yields an unbiased random k -simplex interaction structure without imposing any structural priors.

As an example, the 2-simplex network in Fig. 5C uses $N = 10$. With $p = 0.5$, this produces approximately $0.5 \times \binom{10}{3} \approx 60$ higher-order interactions.

All simulations are implemented in Python using NumPy and SciPy for numerical integration, and PyTorch for automatic differentiation and optimization. Adam or AMSGrad is used for small to intermediate networks, whereas natural gradient descent is employed for large-scale systems. Each experiment is repeated 10–20 times to obtain statistically stable results.

The dynamical experiments in all simulations are conducted using the standard Kuramoto model with unit coupling strength. Natural frequencies ω_i are drawn independently from a uniform distribution over $[-1, 1]$, and each simulation is initialized with random phases sampled uniformly from $[0, 2\pi)$. The full dynamical formulation and numerical implementation details are provided in Supplementary Sec. 1.1.

In all experiments, hyperparameters are chosen to ensure stable and reproducible optimization. Unless stated otherwise, the learning rate is set to $\eta = 5 \times 10^{-3}$ for natural-gradient updates, reflecting their different effective step sizes. The steepness parameter of the sigmoidal ansatz is fixed at $k = 12$, which provides a sharp but numerically stable continuous–binary transition. The residual-sampling ratio is set to $s/N \in [0.03, 0.10]$ depending on network size, ensuring unbiased gradient estimates with low variance.

The regularization parameter for the node-wise weighting term is chosen as $\varepsilon = 10^{-6}$ unless specified otherwise, and the synchronization filtering threshold is set to $\epsilon_{\text{sync}} \in [10^{-4}, 10^{-3}]$. All results are robust to moderate variation of these hyperparameters, and a brief sensitivity analysis is provided in the Supplementary Material.

VI. SUPPLEMENTARY MATERIALS

- S1. Kuramoto model in numerical experiments and dynamical models used to test in Fig. 2B
- S2. Identifiability of Interaction Structures From a Finite Number of Steady States
- S3. Performance on Diverse Network Types, Directed and Weighted Structures
- S4. Comparative Analysis with Classical Reconstruction Methods: Scalability and Identifiability
- S5. Robust identifiability under observational, dynamical, and structural noise
- S6. Computational Efficiency and Scalability: The Role of Residual Sampling and Natural Gradient
- fig. S1. Dependence of the required number of steady states on network density
- fig. S2. Reconstruction across different network topologies
- fig. S3. Directed network reconstruction
- fig. S4. Weighted network reconstruction
- fig. S5. Identifiability comparison on a sparse network

¹A. Arenas, A. Díaz-Guilera, J. Kurths, Y. Moreno, C. Zhou, Synchronization in complex networks, *Physics Reports* 469 (3) (2008) 93–153. doi:10.1016/j.physrep.2008.09.002.

- ²S. H. Strogatz, Exploring complex networks, *Nature* 410 (6825) (2001) 268–276. doi:10.1038/35065725.
- ³A.-L. Barabási, R. Albert, Emergence of scaling in random networks, *Science* 286 (5439) (1999) 509–512.
- ⁴D. J. Watts, S. H. Strogatz, Collective dynamics of ‘small-world’ networks, *Nature* 393 (6684) (1998) 440–442.
- ⁵M. E. Newman, The structure and function of complex networks, *SIAM Review* 45 (2) (2003) 167–256.
- ⁶K. Luo, Z. Cai, Z. Liu, S. Guan, Y. Zou, Effects of uncommon non-isochronicities on remote synchronization (in press), *Chaos, Solitons & Fractals* 181 (2024) 114705.
- ⁷S. H. Strogatz, D. J. Watts, M. E. Newman, A comparative review of network reconstruction methods, *Nature Reviews Physics* 3 (12) (2021) 718–737.
- ⁸M. Timme, Revealing network connectivity from response dynamics, *Physical Review Letters* 98 (22) (2007) 224101.
- ⁹E. D. Sontag, Network reconstruction from data using differential equations, *ASME Journal of Dynamic Systems, Measurement, and Control* 130 (3) (2008) 031001.
- ¹⁰Y. Yuan, S. Stanhope, B. Ermentrout, D. Nykamp, Robust dynamical network structure reconstruction, *Physical Review E* 84 (2) (2011) 026102.
- ¹¹T. Carletti, F. Battiston, G. Cimini, D. Fanelli, Inferring hypergraphs from dynamics on networks, *Nature Communications* 11 (1) (2020) 4726.
- ¹²Y. Wang, Z. Yuan, J.-A. Lu, J. Kurths, Robust network reconstruction from noisy time series with hidden nodes, *Chaos* 30 (9) (2020) 093106.
- ¹³A. J. Gates, I. B. Wood, W. P. Hetrick, Y.-Y. Ahn, Network reconstruction under partial observability and noise, *Science Advances* 8 (5) (2022) eabj2432.
- ¹⁴L. Barnett, J. T. Lizier, M. Harré, A. K. Seth, Sparse and robust network inference from noisy data via ℓ_1 -regularization, *Physical Review E* 95 (5) (2017) 052315.
- ¹⁵M. Nitzan, J. Casadiego, M. Timme, Revealing physical interaction networks from statistics of collective dynamics, *Science Advances* 3 (2) (2017) e1600396.
- ¹⁶S. G. Shandilya, M. Timme, Inferring network topology from complex dynamics, *New Journal of Physics* 13 (1) (2011) 013004.
- ¹⁷D. Yu, U. Parlitz, Driving a network to steady states reveals its cooperative architecture, *Europhysics Letters* 81 (4) (2008) 48007.
- ¹⁸D. Napolitano, T. Sauer, Reconstructing the topology of sparsely connected dynamical networks, *Physical Review E* 77 (2) (2008) 026103.
- ¹⁹W.-X. Wang, R. Yang, Y.-C. Lai, V. Kovanis, C. Grebogi, Predicting catastrophes in nonlinear dynamical systems by compressive sensing, *Physical Review Letters* 106 (15) (2011) 154101.
- ²⁰T. Schreiber, Measuring information transfer, *Physical Review Letters* 85 (2) (2000) 461–464.
- ²¹S. Tajima, T. Yanagawa, N. Fujii, T. Toyozumi, Untangling brain-wide dynamics in consciousness by cross-embedding, *PLOS Computational Biology* 11 (11) (2015) e1004537.
- ²²S. L. Brunton, J. L. Proctor, J. N. Kutz, Discovering governing equations from data by sparse identification of nonlinear dynamical systems, *Proceedings of the National Academy of Sciences* 113 (15) (2016) 3932–3937.
- ²³K.-M. Luo, S.-G. Guan, Y. Zou, Reconstruction of simplex structures based on phase synchronization dynamics, *Acta Physica Sinica* 73 (12) (2024) 120501.
- ²⁴M. Cranmer, A. Sanchez-Gonzalez, P. Battaglia, R. Xu, K. Cranmer, Physics-informed graph networks for learning dynamical systems, in: *International Conference on Machine Learning*, PMLR, 2020, pp. 3242–3251.
- ²⁵M. Raissi, P. Perdikaris, G. E. Karniadakis, Physics-informed neural networks: A deep learning framework for solving forward and inverse problems involving nonlinear partial differential equations, *Journal of Computational Physics* 378 (2019) 686–707. doi:10.1016/j.jcp.2018.10.045.
- ²⁶G. E. Karniadakis, I. G. Kevrekidis, L. Lu, P. Perdikaris, S. Wang, L. Yang, Physics-informed machine learning, *Nature Reviews Physics* 3 (6) (2021) 422–440.
- ²⁷I. E. Lagaris, A. Likas, D. I. Fotiadis, Artificial neural networks for solving ordinary and partial differential equations, *IEEE Transactions on Neural Networks* 9 (5) (1998) 987–1000.
- ²⁸T. P. Peixoto, Bayesian inference of network structure from data, *Physical Review Letters* 123 (12) (2019) 128301.
- ²⁹T. P. Peixoto, Network reconstruction via the minimum description length principle (in press), *Phys. Rev. X* 15 (2025) 011065.
- ³⁰S. Feizi, D. Marbach, M. Médard, M. Kellis, Network deconvolution as a general method to distinguish direct dependencies in networks, *Nature Biotechnology* 31 (8) (2013) 726–733.
- ³¹B. Schelter, M. Winterhalder, R. Dahlhaus, J. Kurths, J. Timmer, Partial phase synchronization for multivariate synchronizing systems, *Physical Review Letters* 96 (20) (2006) 208103.
- ³²B. N. Kholodenko, A. Kiyatkin, F. J. Bruggeman, E. D. Sontag, H. V. Westerhoff, J. B. Hoek, Untangling the wires: a strategy to trace functional interactions in signaling and gene networks, *Proceedings of the National Academy of Sciences* 99 (20) (2002) 12841–12846.
- ³³B. Barzel, A.-L. Barabási, Network link prediction by global silencing of indirect correlations, *Nature Biotechnology* 31 (8) (2013) 720–725.
- ³⁴R. A. Rossi, N. K. Ahmed, The network data repository with interactive graph analytics and visualization, in: *AAAI*, 2015.
- ³⁵P. Hagmann, L. Cammoun, X. Gigandet, R. Meuli, C. J. Honey, V. J. Wedeen, O. Sporns, Mapping the structural core of human cerebral cortex, *PLoS Biology* 6 (7) (2008) e159.
- ³⁶K. Luo, Hierarchical synchronization and distortion scaling in social media networks: A fractal-like topology theory, *Chaos, Solitons & Fractals* 202 (2026) 117581.